PCCP

PAPER

A new generation of platinum and iodine free efficient dye-sensitized solar cells†

Shahzada Ahmad,[*ab] **Takeru Bessho,**[a] **Florian Kessler,**[a] **Etienne Baranoff,**[a] **Julien Frey,**[a] **Chenyi Yi,**[a] **Michael Grätzel**[a] **and Mohammad K. Nazeeruddin**[*a]

We report a series of cobalt complexes with various polypyridyl ligands, where the oxidation potential is tuned from 0.17 to 0.34 V *vs.* ferrocene. The highest occupied molecular orbitals (HOMO) of the cobalt complexes were stabilized by adding electron acceptor groups on pyridyl or replacing pyridyl by pyrazole. These complexes are then used as one-electron redox mediators in dye sensitized solar cells (DSSCs) together with polymer based cathode resulting in an excellent performance. The performance of DSSCs using the molecularly engineered cobalt redox shuttle and poly(3,4-alkylthiophenes) based cathode is better than the triiodide/iodide redox shuttle with platinized cathode. The use of high surface area poly(3,4-propylenedioxythiophene) based nanoporous layers allows higher catalytic activity thus minimizing the electrode–electrolyte interface issues.

1. Introduction

An energy source, which is green and can counter our global warming process, is one of the main research topics in the present scenario. In this context dye sensitized solar cells (DSSCs) are now being exploited as one of the available alternatives owing to their numerous advantages.[1,2] DSSCs are composed of a mesoporous network of TiO_2 nanocrystals anchored with sensitizer, and a platinized current collector sandwiched with redox electrolyte. Several groups have explored photoanode materials and sensitizers,[1–4] while triiodide/iodide based redox couples with platinized cathodes have remained indispensable for almost two decades in the fabrication of efficient DSSCs. The development of new redox couples and counter electrodes is the paramount research in the process of making DSSCs the undisputed choice for a clean and cheap energy source.[5,6] The counter electrode is one of the vital components, which reduces the oxidized redox mediator, generated after the dye regeneration. Since transparent conductive oxide (TCO) substrates exhibit insufficient electron transfer kinetics for I_3^- reduction, a thin layer of Platinum (Pt) is coated onto the TCO substrate (platinized cathode) and is used to catalyse the cathodic reduction of I_3^- ions, *i.e.* redox couple regeneration.[7] However both these

components of DSSCs suffer from their inability in long-term reliability. The I_3^-/I^- based electrolyte is corrosive, yellow in color and dissipative towards light absorption, while platinized cathode is subject to corrosion, sensitive to side products formation, and liable to become inactivated with ageing, apart from being uneconomical. These are major attributes which may limit the use of I_3^-/I^- based electrolytes and Pt in some cases. This is considered as a realm of scientific potential in the DSSCs fabrication. After the seminal work on the use of cobalt electrolytes in DSSCs[8] recently renewed attention has been given and polypyridyl cobalt redox complexes have been explored.[9–13] The attempts to replace the I_3^-/I^- redox shuttle by cobalt polypyridine complexes was not only limited to their low visible light absorption but also due to their higher redox potential and noncorrosive nature towards cathode. At full sun (AM 1.5 GM) the performance of cobalt complexes as redox shuttles is diffusion limited and also a faster back reaction of photo-injected electrons with the oxidized species is expected. As a matter of fact, until recently hardly any electron outer-sphere redox couples have been demonstrated in making efficient cells, with a power conversion efficiency (PCE) comparable to the I_3^-/I^- based redox couples, to complement its use. In 2010 Feldt *et al*. reported an increased PCE of 6.7% by employing a syngerstic D-π-A organic sensitizer (**D35**) in conjunction with $[Co^{III}(bpy)_3](PF_6)_3/$$[Co^{II}(bpy)_3](PF_6)_2$ redox shuttle,[13] and this was also the subject of a recent review.[14] We have also demonstrated a PCE of 10% with a dye, called **Y123**, and $[Co^{III}(bpy)_3](B(CN)_4)_3/$$[Co^{II}(bpy)_3](B(CN)_4)_2$ redox couple.[15,16] Since the studied cobalt complexes used so far were based on simple bipyridine and phenanthroline ligands we exploited various new cobalt

a Laboratory of Photonics and Interfaces, Department de Chimie, Ecole Polytechnique Federale de Lausanne, CH-1015 Lausanne, Switzerland. E-mail: mdkhaja.nazeeruddin@epfl.ch; Fax: 41216934111; Tel: 41216936124

b Max Planck Institute for Polymer Research, Ackermannweg 10, D-55138 Mainz, Germany. E-mail: ahmad@mpip-mainz.mpg.de

† Electronic supplementary information (ESI) available: cyclic voltammetry of redox couples. See DOI: 10.1039/c2cp41611e

complexes with higher oxidation potentials (0.81 to 0.98 V *vs.* NHE) than $[Co(bpy)_3]$ (0.56 V *vs.* NHE) and $[Co(phen)_3]$ (0.62 V *vs.* NHE) complexes. This allows us to define the driving force required to regenerate the dye. Additionally we describe the influence of different counter ions for the cobalt complexes on the photovoltaic (PV) performance. High V_{oc} values of up to 1000 mV were obtained due to the inherent higher positive potential as compared to the I_3^-/I^- redox shuttle.

We have learned that the conventional platinized cathode is not optimal with these newly developed redox shuttles, so to overcome this barrier, a series of poly(3,4-alkylthiophenes) members were exploited as a cathode in DSSCs. These counter electrodes were then fine tuned with the use of various dopants for their physico–chemical properties to be used in DSSCs. Poly(3,4-propylenedioxythiophene) [PProDOT] based DSSCs exhibit excellent results due to their ultra high surface area morphology and lack of the possibility of forming any passivation layer at the electrode–electrolyte interface. These polymer cathodes were then studied for their compatibility with the formulated noncorrosive cobalt (III/II) based redox shuttle. Herein we demonstrate efficient Pt-free and iodine-free DSSCs fabrication in conjunction with our rationally designed high molar extinction coefficient organic D-π-A sensitizer, 3-{6-{4-[bis(2′,4′-dihexyloxybiphenyl-4-yl)amino-]phenyl}-4,4-dihexyl-cyclo-penta-[2,1-b:3,4-b′]dithiophene-2-yl}-2-cyanoacrylic acid (labelled as **Y123**).[15]

2. Results and discussion

2.1 Redox-shuttle

The cobalt complexes as well as the structure of the organic dye used in this study are shown in Scheme 1. As reported by us, the complex **4a** $[Co(bpy-pz)_2]^{2+}$ has a standard redox potential of 0.22 V *versus* ferrocenium/ferrocene (Fc^+/Fc).[5] For complexes **5a** and **6a** bearing the same tridentate ligand as of complex **4a** but with different anions such as tetracyanoborate (**5a**) and bis(trifluoromethanesulfonyl)imide (**6a**) instead
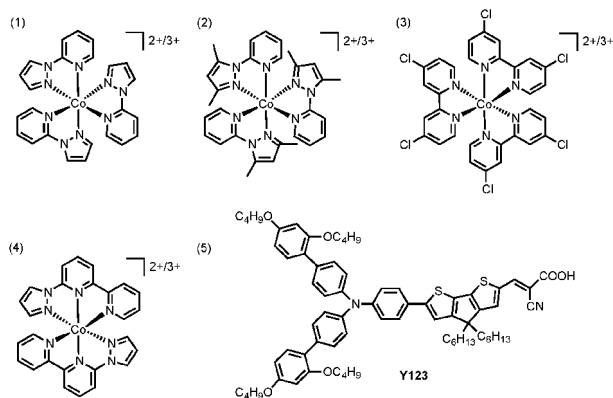
Scheme 1 Structures of the redox shuttles and organic dye (1) $[Co(py-pz)_3](PF_6)_2$ (1a), $[Co(py-pz)_3](PF_6)_3$ (1b); (2) $[Co(py-pzMe_2)_3](PF_6)_2$ (2a), $[Co(py-pzMe_2)_3](PF_6)_3$ (2b); (3) $[Co(Cl_2bpy)_3](PF_6)_2$ (3a), $[Co(Cl_2bpy)_3](PF_6)_3$ (3b); (4) $[Co(bpy-pz)_2](PF_6)_2$ (4a), $[Co(bpy-pz)_2]$-$(PF_6)_3$ (4b), $[Co(bpy-pz)_2](B(CN)_4)_2$ (5a), $[Co(bpy-pz)_2](B(CN)_4)_3$ (5b), $[Co(bpy-pz)_2](TFSI)_2$ (6a), $[Co(bpy-pz)_2](TFSI)_3$ (6b); (5) organic dye called **Y123**.

Table 1 Oxidation and reduction potentials (V *vs.* ferrocene) of compounds as obtained from cyclic voltammetry ($E = \frac{1}{2}$(Epa + Epc); acetonitrile/TBAPF$_6$ 0.1 M, *vs.* Fc + /Fc)

	1a	2a	3a	4a	5a	6a
Oxidation (V)	0.32	0.34	0.17	0.22	0.23	0.24
Reduction (V)	−1.45	−1.55	−1.15	−1.20	−1.20	−1.20

of hexafluorophosphate (**4a**), as expected a rather similar potential was obtained (Table 1). In spite of the similar redox potential, these complexes which were studied as the counter ion may influence the diffusion and solubility properties and therefore the device performance. Complex **4a** was used as a benchmark due to its excellent device performance, and to optimize the system additional complexes were designed with slightly lower (**3a**) and slightly higher oxidation potentials (**1a** and **2a**). Complex **3a** is based on a 4,4′-dichloro-2,2′-bipyridine ligand[17] and is easily accessible due to its commercial availability. The higher oxidation potential of complex **1a** in contrast to complex **4a** is attributed to the presence of one additional pyrazole, which stabilizes the highest occupied molecular orbital (HOMO) of the complex more than a pyridine group. This results in a higher oxidation potential by 100 mV. Additional weakly donating substituents (methyl groups) on the backbone of the ligand in complex **2a** result in a slight increase of the standard potential to 0.34 V *vs.* ferrocenium/ferrocene. The ligands of complexes **1a** and **2a** were synthesized by a simple one step method using 2-fluoro-pyridine and pyrazole or 3,5-dimethylpyrazole.

2.2 Counter electrodes

The electro-polymerized films of PProDOT exhibit homogeneous nanoporous morphologies with uniform grain size. Platinum forms monocrystalline small granules, while Fig. 1(a–d) show highly porous structures. Polymer films grown in other media show mainly compact granular structures. Scheme 2 shows the structure of the monomers employed for the polymerization process. These nanoporous polymers with ultra-high surface areas are ideal candidates for electro-catalysis and are also envisioned as materials for the oxygen reduction reaction.[18] The use of nanoporous polymer films will allow the post functionalization of the pore walls with the redox shuttle without forming any passivation layer at the electrode–electrolyte interface. The obtained highly porous microstructure was possible due to the use of room temperature ionic liquids (RTILs), which not only work as a supporting electrolyte in the synthesis of polymers but also have influence to totally alter reaction pathways and product microstructures due to their hydrophobicity.[19] With the proper choice of ionic liquids employed, the shape and pore size of a material can be tuned and it evolves from one form to another with varying pore diameter. With the change of anion in the RTILs, the microstructure changes from small fibril shapes to elongated fibril to sponge like morphology Fig. 1(d).

Due to the different hydrophobicity of the surface, the contact angles for PProDOT grown in BMPyTFSI and EMI-FAP are 120 and 112, respectively. The distinct morphologies obtained with the use of RTILs is due to the insertion of both cation and anion in the polymer matrix.[19] During the
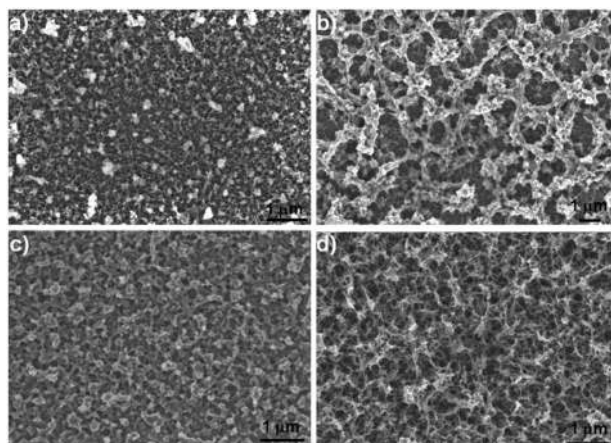
Fig. 1 SEM images of (a) PProDOT[BMPyTFSI], (b) PProDOT-[EMIFAP], (c) PProDOT[BMITFSI], (d) PProDOT[EMITCB]. The abbreviation in the parentheses identifies the ionic liquid used.
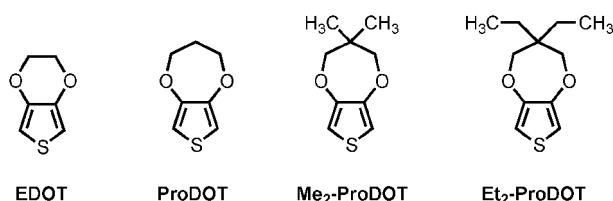

Scheme 2 Chemical structures of the different compounds used as monomers for polymerization.

electro-polymerization, anions are incorporated into the polymer matrix as dopants and this dictates the growth pattern (due to viscosity of medium and diffusion limitation). Polymer films synthesized in the presence of TFSI$^-$ as the anion exhibit relatively rigid fibers connected with granular shapes. The change of cation from pyridinium to imidazolium also induces large variation in the microstructure, which further supports the hypothesis of insertion of both cation and anion when RTILs are used. The TFSI$^-$ anion posseses a relatively large structure with a diffuse negative charge on a nitrogen atom due to electron withdrawing groups and results in a larger mesh size in the microstructure compared to the tetracyanoborate anions which gave more soft and smaller pores.

Conductive scanning force microscopy (CSFM) was performed to evaluate the homogeneities of current at nanoscale, this allows simultaneous measurement of topography and the variation of current on the application of an electrode bias. Fig. 2a shows the topographical image of PProDOT1, and also illustrates the highly porous structure as obtained from the scanning electron microscope. The root mean square (RMS) roughness of films was estimated on a 2.5 × 2.5 μm^2 scale and under our conditions we found a RMS roughness value of 34 nm of a film with thickness of 500 nm. The mapping of the current illustrates large domains of current with a high conductance value. The dialkoxy substituents minimize the possible synthetic defects, and due their electron donating nature improving the conductivity.

The presence of a porous structure limits the uniform distribution of current and mostly induces large domains of
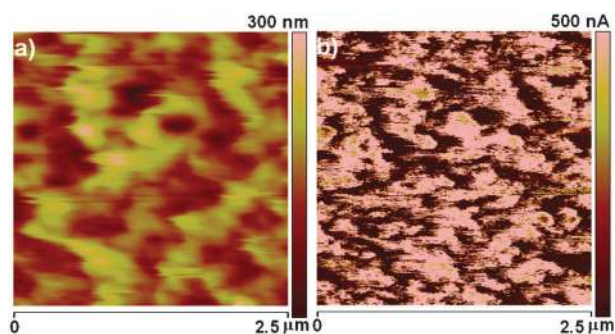
Fig. 2 CSFM images of (a) topography (b) current at a bias of 100 mV.

conductance. However we assume that in spite of this charge transfer by intra polaronic islands it is also occurring at the bottom of the electrode, as the polymers grow from nucleation and growth phenomena. Due to the highly porous network higher resolution images were not possible with CSFM. The average RMS value of current in these layers is 350 nA while the maximum obtained current is 900 nA at an applied bias of 100 mV. The bright features in the images correspond to the grains of higher conductance compared to the surrounding. The conductivity of the polymers depends on the water content as well as the conductivity of the polymerizing bath. RTILs are hydrophobic and may also expel any water product formation, thus minimizing the defects at the nanometer scale during polymerization and mostly giving a uniform distribution unlike classical electrolytes which form islands of non-conducting domains.[20]

2.3 Photovoltaic performance

The DSSCs were fabricated using the **Y123** sensitizer,[15] cobalt redox shuttles, and poly(3,4-alkylthiophenes) as cathodes. The fabricated cells exhibit broad incident photon-to-current conversion efficiencies (IPCE) almost plateau like from 450–650 nm with high IPCE maxima > 90% (Fig. 3), which is higher when compared to the cells with I_3^-/I$^-$[21] and other reports of cobalt complex, and reached near to unity.

A cobalt based redox shuttle stained the titania films with an enhanced photocurrent response in the spectral range from 390–470 nm compared to the I_3^-/I$^-$ based system due to lower absorption coefficients in the blue region and give high V_{oc}. All polymer based cathode showed similar incident IPCE. The PV performance using the **4a,b** redox shuttle showed a maximum short circuit photocurrent density (J_{sc}) of 12.6 mA cm^{-2}, 1000 mV open circuit potential (V_{oc}) and a fill factor (FF) of ∼0.78 resulting in ∼9.9% power conversion efficiency (η) at standard global AM 1.5 solar conditions (Fig. 4b) with PPro-DOT1. Under the same conditions, the efficiency using a platinized cathode is illustrated in Fig. 4a, which under-performed. Most of the devices showed a linear response of J_{sc} and a slightly higher η under a lower light intensity due to a higher fill factor, which is ascribed to a lower ohmic loss (Table 2).

Different V_{oc} and J_{sc} values were obtained depending on the redox shuttle (Tables 2–7). For complex **1a,b** (Table 2) the low performance of the devices is due to the high oxidation potential of the redox shuttle which is too close to the
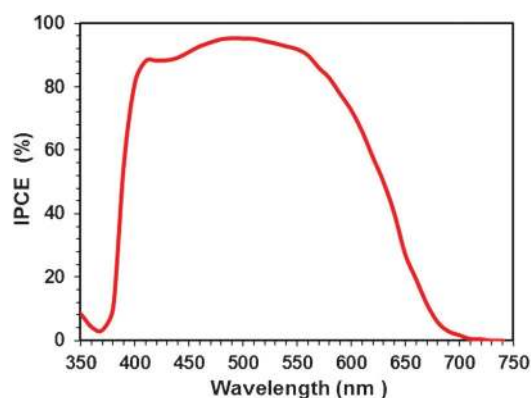
Fig. 3 The incident photon-to-electron-conversion efficiency (IPCE) as function of wavelength of monochromatic light for PProDOT1 based counter electrodes by using **4a,b** as a redox couple under standard illumination conditions (AM 1.5 G, 100 mW cm^{-2}).
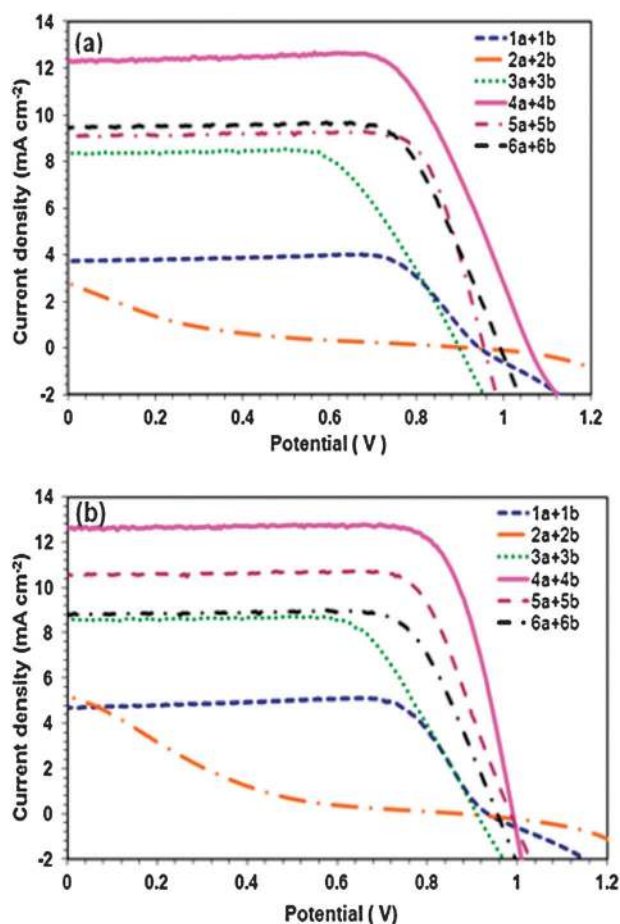
Fig. 4 J–V characteristics of DSSCs employing various cobalt based redox shuttles (a) with Pt and (b) with PProDOT1 as a counter electrode under 100 mW cm^{-2} illumination (AM 1.5 G).

oxidation potential of the dye resulting in slow dye regeneration, therefore low current was obtained, especially under full sun. With the use of PEDOT and PProDOT2 the FF is lower compared to the platinized cathode while a rather similar V_{oc} is observed. However, this loss in FF is overcompensated by the higher current obtained with these polymeric cathodes

Table 2 Photovoltaic parameters at different light intensities with redox shuttle **1a,b**

	PV Parameters	Pt	PEDOT	PProDOT1	PProDOT2
0.1 Sun	V_{sc} (mV)	871	867	860	874
	J_{sc} (mA cm^{-2})	0.53	1.0	0.68	0.95
	FF	0.88	0.76	0.85	0.76
	η (%)	4.37	7.15	5.39	7.05
0.5 Sun	V_{oc} (mV)	930	946	923	943
	J_{sc} (mA cm^{-2})	2.3	4.4	2.95	4.91
	FF	0.83	0.66	0.83	0.70
	η (%)	3.49	5.44	4.45	5.45
1 Sun	V_{oc} (mV)	943	954	934	949
	J_{sc} (mA cm^{-2})	3.74	7.13	4.70	6.64
	FF	0.80	0.53	0.81	0.65
	η (%)	2.81	3.66	3.59	4.1

and the overall efficiency was increased by 46% (from 2.81% to 4.1%) under full sunlight with the change of cathode from Pt to PProDOT2. PProDOT1 gave similar FF to the reference platinized cathode and a slight increase in current resulting in an intermediate performance.

Table 3 summarizes the PV results obtained with redox shuttle **2a,b**. The oxidation potential of **2a** is even higher than that of complex **1a** and the driving force to regenerate the dye is almost negligible. Surprisingly this small difference in oxidation potential by 20 mV resulted in a drastically lower device performance, pointing towards the conclusion that the driving force of less than 100 mV for dye regeneration is insufficient. Drastically lower FF and J_{sc} were obtained, which get better with the use of polymer cathodes (250% increase) but are still not optimum for device application.

The oxidation potential of complex **3a** is 150 mV lower than that of complex **1a** (Table 1). This additional driving force for dye regeneration translates into the higher short circuit current of the devices as depicted in Table 4. As expected, the V_{oc} was slightly lower compared to the devices using the **1a,b** redox shuttle. But the over all efficiency still remains higher and with the proper choice of cathodes, the device performance improved to 5.57% efficiency. Exceptionally high V_{oc} and best performing devices were obtained when complexes **4a,b** were employed as the redox shuttle (Table 5). This excellent performance is attributed to a perfect match between the oxidation potential of the dye and the redox shuttle. An additional asset is the good reversibility of oxidation of this redox shuttle (see ESI† for CV).

Table 3 Photovoltaic parameters at different light intensities with redox shuttle **2a,b**

	PV Parameters	Pt	PEDOT	PProDOT1	PProDOT2
0.1 Sun	V_{oc} (mV)	808	797	831	729
	J_{sc} (mA cm^{-2})	0.95	0.96	0.89	0.92
	FF	0.20	0.19	0.3	0.22
	η (%)	1.65	1.61	2.36	1.97
0.5 Sun	V_{oc} (mV)	893	827	878	793
	J_{sc} (mA cm^{-2})	2.47	3.54	3.42	3.46
	FF	0.11	0.13	0.19	0.15
	η (%)	0.48	0.73	1.1	0.82
1 Sun	V_{oc} (mV)	908	831	873	802
	J_{sc} (mA cm^{-2})	2.77	4.96	5.15	4.75
	FF	0.10	0.11	0.14	0.13
	η (%)	0.27	0.47	0.65	0.49

Table 4 Photovoltaic parameters at different light intensities with redox shuttle **3a,b**

	PV Parameters	Pt	PEDOT	PProDOT1	PProDOT2
0.1 Sun	V_{oc} (mV)	808	835	823	712
	J_{sc} (mA cm^{-2})	1.1	1.3	1.1	0.94
	FF	0.73	0.66	0.72	0.78
	η (%)	6.9	7.63	6.88	5.52
0.5 Sun	V_{oc} (mV)	876	892	889	785
	J_{sc} (mA cm^{-2})	5.23	6.3	5.28	4.52
	FF	0.67	0.63	0.70	0.74
	η (%)	6.04	6.87	6.35	5.15
1 Sun	V_{oc} (mV)	897	911	910	809
	J_{sc} (mA cm^{-2})	8.32	10.14	8.57	7.66
	FF	0.65	0.60	0.68	0.71
	η (%)	4.85	5.57	5.27	4.39

Table 5 Photovoltaic parameters at different light intensities with redox shuttle **4a,b**

	PV Parameters	Pt	PEDOT	PProDOT1	PProDOT2
0.1 Sun	V_{oc} (mV)	909	931	914	911
	J_{sc} (mA cm^{-2})	1.23	1.33	1.29	1.35
	FF	0.79	0.74	0.82	0.77
	η (%)	9.38	9.74	10.24	10.03
0.5 Sun	V_{oc} (mV)	984	1000	978	980
	J_{sc} (mA cm^{-2})	6.21	6.76	6.87	6.80
	FF	0.76	0.71	0.80	0.75
	η (%)	9.14	9.4	10.45	9.69
1 Sun	V_{oc} (mV)	1001	1027	999	1003
	J_{sc} (mA cm^{-2})	11.03	12.15	12.62	11.95
	FF	0.74	0.69	0.78	0.73
	η (%)	8.24	8.62	9.9	8.7

Under full sun illumination, $V_{oc} > 1000$ mV was observed, together with a high current of 11 mA and a FF of 0.74 resulting an overall efficiency of 8.24% for the device with platinized cathode. The cells with PEDOT, PProDOT1, and PProDOT2 counter electrodes yielded an improvement of an additional 20% in efficiency (9.9%). A remarkable drop in charge transfer resistance (2.5 Ω cm^{-2}) was observed[5] when PProDOT1 was used as compared to the platinized cathode (50 Ω cm^{-2}), pointing towards a favorable electrode–electrolyte interface.

When the PF_6^- anion in complex **4a,b** was replaced by $B(CN)_4^-$ (**5a,b**; Table 6) and $TFSI^-$ (**6a,b**; Table 7) a drop in both V_{oc} and J_{sc} was observed. However in the case of $B(CN)_4^-$ the polymer cathode was further able to improve

Table 6 Photovoltaic parameters at different light intensities with redox shuttle **5a,b**

	PV Parameters	Pt	PEDOT	PProDOT1	PProDOT2
0.1 Sun	V_{oc} (mV)	856	870	867	860
	J_{sc} (mA cm^{-2})	0.99	1.36	1.18	1.16
	FF	0.82	0.74	0.81	0.81
	η (%)	7.37	9.27	8.77	8.62
0.5 Sun	V_{oc} (mV)	929	951	958	936
	J_{sc} (mA cm^{-2})	5.19	6.86	6.02	6.06
	FF	0.80	0.69	0.77	0.77
	η (%)	7.59	8.75	8.64	8.54
1 Sun	V_{oc} (mV)	955	975	986	960
	J_{sc} (mA cm^{-2})	9.13	12.13	10.58	10.73
	FF	0.79	0.65	0.74	0.75
	η (%)	6.87	7.68	7.72	7.7

Table 7 Photovoltaic parameters at different light intensities with redox shuttle **6a,b**

	PV Parameters	Pt	PEDOT	PProDOT1	PProDOT2
0.1 Sun	V_{oc} (mV)	875	862	848	857
	J_{sc} (mA cm^{-2})	1.14	1.27	1.03	1.13
	FF	0.79	0.72	0.79	0.79
	η (%)	8.32	8.32	7.36	8.05
0.5 Sun	V_{oc} (mV)	966	933	930	929
	J_{sc} (mA cm^{-2})	5.71	6.17	5.21	5.63
	FF	0.75	0.67	0.75	0.75
	η (%)	8.04	7.54	7.15	7.65
1 Sun	V_{oc} (mV)	992	955	955	952
	J_{sc} (mA cm^{-2})	9.46	10	8.85	9.51
	FF	0.73	0.64	0.74	0.74
	η (%)	6.78	6.11	6.2	6.6

the J_{sc} and efficiency. The relatively large size of $TFSI^-$ in (complex **6a,b**) come as an obstacle in its path to compete for better PV properties (Table 7). The observed loss in V_{oc} of polymer cathode devices is ascribed to the redox shuttle/polymer and/or the electrical sheet resistance at the interface of the FTO/polymer. A similar observation was found when an I_3^-/I^- redox shuttle was used for DSSCs fabrication.[22,23] In all the cobalt complexes, the PProDOT cathode showed comparable or enhanced V_{oc} to platinized cathode. The redox shuttles using PProDOT2 as cathode exhibit a drop in both J_{sc} and V_{oc}. A lower V_{oc} states a downward shift of the band edge toward more positive potentials.[24]

The band edge shift is ascribed to the redox shuttle composition, surface modification of semiconducting particles,[22,24] etc. The possible surface modification medium here is RTILs used during the electrodeposition, and complete removal by washing is rather tricky. As a consequence, the RTIL species will be miscible with the redox shuttle and may influence the band edge after diffusion and adsorption to the TiO$_2$ surface. Another plausible reason is the storage of charge in these redox active materials, when came in contact with the electrolytes, and for this reason they enjoy the privilege of being probed for supercapacitors.[25] The role of counter ion in the polymer matrix has an influence on both the V_{oc} and J_{sc} of the devices, mainly due to the different porosity, conductivity and thickness of the films.

With an aim to further induce flexibility in the polymer chain, dialkyl substituents in the PProDOT ring were exploited in combination with our best complex, **4a,b** (Table 8). The use of dialkyl groups as a side chain in PProDOT, lowers the FF value, which originates from the relatively lower conductivity of the polymer. However it was able to improve the J_{sc} and resulted in a higher PCE than that of the platinized cathode. We conclude that the more bulky group results in a slower mass diffusion process.

Fig. 5 summarize the result obtained with the thickness variation of polymer cathodes. The thickness of the polymer films can easily be tuned by varying the polymerization time. With the increase in polymerization time, as expected, there is a steep growth in the thickness of polymer films, while to a larger extent the PV properties remain same in the measured window. We have noted that to be used as an efficient cathode in DSSCs a ∼500 nm thick PProDOT film is optimum for applications.

Table 8 Photovoltaic parameters at different light intensities with redox shuttle **4a,b** for PProDOT derivatives

	PV Parameters	Pt	Me₂-PProDOT	Et₂-PProDOT
0.1 Sun	V_{oc} (mV)	909	924	928
	J_{sc} (mA cm^{-2})	1.23	1.31	1.29
	FF	0.79	0.79	0.80
	η (%)	9.38	10.23	10.19
0.5 Sun	V_{oc} (mV)	984	988	988
	J_{sc} (mA cm^{-2})	6.21	6.87	6.56
	FF	0.76	0.73	0.73
	η (%)	9.14	9.75	9.27
1 Sun	V_{oc} (mV)	1001	1006	1006
	J_{sc} (mA cm^{-2})	11.03	12.33	11.51
	FF	0.74	0.70	0.70
	η (%)	8.24	8.74	8.0
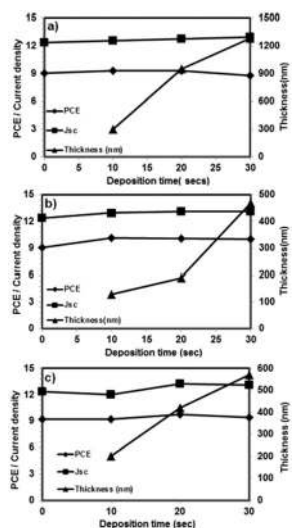
Fig. 5 Photovoltaic parameters as a function of thickness of (a) PEDOT[BMITFSI], (b) PProDOT[BMITFSI] and (c) PProDOT-[EMIFAP] using **4a,b** as redox shuttle. The 0 on the X-axis refers to platinized cathode.

3. Experimental section

3.1 Materials

1-butyl-3-methylimidazolium bis(trifluoromethylsulfonyl)imide, (BMITFSI) and 1-butyl-3-methylpyridinium bis(trifluoromethylsulfonyl)imide (BMPyTFSI) were obtained from IoLiTec GmbH, while 1-ethyl-3-methylimidazolium tris(pentafluoroethyl) trifluorophosphate (EMIFAP) and 1-ethyl-3-methylimidazolium tetracyanoborate (EMITCB) were obtained from Merck KGaA and of ultrapure quality. 3,4-ethylenedioxy-thiophene (EDOT) was of Baytron, MV-2 grade, while 3,4-propylenedioxythiophene (ProDOT), 3,4-(2′,2′-dimethyl-propylene)-dioxythiophene (Me₂-ProDOT) and 3,4-(2′,2′-diethylpropylene)-dioxythiophene (Et₂-ProDOT) monomers were obtained from Sigma-Aldrich and used as received. Cobalt chloride hexahydrate was purchased from Fluka and 4,4′-dichloro-2,2′-bipyridine (Cl₂bpy) from Ace Synthesis. 2-(1H-pyrazol-1-yl)pyridine (py-pz), [Co(py-pz)₃](PF₆)₂ (**1a**), [Co(py-pz)₃](PF₆)₃ (**1b**),[23] 6-(1H-pyrazol-1-yl)-2,2′-bipyridine (bpy-pz), [Co(bpy-pz)₂](PF₆)₂ (**4a**), [Co(bpy-pz)₂](PF₆)₃ (**4b**)[5] were prepared according to literature procedures.

2-(3,5-dimethyl-1H-pyrazol-1-yl)pyridine (py-pzMe₂) was prepared in a similar manner to the synthesis of py-pz.[26] All other materials and solvents were of reagent quality and were used as received.

3.2 Synthesis of redox shuttles

[Co(py-pzMe₂)₃](PF₆)₂ (2a). 520 mg (3.0 mmol, 3.0 eq) of 2-(1H-pyrazol-1-yl)pyridine (py-pz) were dissolved in a 2:1 mixture of water and MeOH (20 mL/10 mL) and then heated to 70 °C. 238 mg (1.0 mmol, 1 eq) of CoCl₂·6H₂O was added as a solid. The mixture was stirred at 70 °C for 10 min and then 0.92 g KPF₆ dissolved in 20 mL of hot water was added. After cooling to r. t. the precipitate was collected on a sintered glass frit, washed with water and Et₂O and dried in vacuo. The pure product (pink solid) was obtained as mixture of mer- and fac-isomers. Yield: 737 mg (0.85 mmol, 85%). HRMS (ESI-TOF) m/z (%): calcd for C₃₀H₃₁CoN₉. 289.1096; found 289.1091 (100) [(M + 2H − 2PF₆)$^{2+}$]. Anal. Calcd. for C₃₀H₃₃CoF₁₂N₉P₂ (868.51): C 41.49, H 3.83, N 14.51; found: C 40.69, H 3.86, N 13.56%.

[Co(py-pzMe₂)₃](PF₆)₃ (2b). 1.04 g (6.0 mmol, 3.0 eq) of 2-(1H-pyrazol-1-yl)pyridine (py-pz) was dissolved in a 2:1 mixture of water and MeOH (40 mL/20 mL) and then heated to 70 °C. 476 mg (2.0 mmol, 1 eq) of CoCl₂·6H₂O was added as a solid. The mixture was stirred at 70 °C for 10 min and then 5 mL of H₂O₂ (30%) and 5 mL of HCl (37%) were added and the mixture was stirred at 70 °C for a further 3h. Excess of aq. KPF₆ solution was added. After cooling to r. t. the precipitate was collected on a sintered glass frit, washed with water and Et₂O and dried in vacuo. The pure product was obtained as an orange solid. Yield: 100 mg (0.1 mmol, 5%). ^{19}F NMR (188 MHz, acetone-D6): δ −72.6 (d, $^{1}J_{PF}$ = 706 Hz, PF₆) ppm. HRMS (ESI-TOF) m/z (%): calcd. for C₃₀H₃₃CoN₉P₂F₁₂ 868.1475; found 868.1669 (100) [(M − PF₆)$^{+}$].

[Co(Cl₂bpy)₃](PF₆)₂ (3a). 238 mg (1.0 mmol, 1 eq) of CoCl₂·6H₂O was dissolved in 15 mL of water and 675 mg (3.0 mmol, 3 eq) of 4,4′-dichloro-2,2′-bipyridine, dissolved in 50 mL of acetone, was added. The solution instantly turned orange and was heated to 50 °C for 10 min. The mixture was concentrated until precipitation occurred. Then the mixture was heated to 50 °C again and just enough acetone was added to re-dissolve the precipitate. Excess of saturated aq. KPF₆ solution was added to precipitate the complex as its PF₆ salt. The solid was collected on a glass-frit, washed with water and Et₂O and dried in air at 90 °C and then in vacuo. The product was obtained as a beige solid. Yield: 950 mg (0.93 mmol, 93%). ^{1}H NMR (400 MHz, acetone-D6): δ 90.11 (s, 6H, ArH), 80.97 (s, 6H, ArH), 42.25 (s, 6H, ArH) ppm. ^{19}F NMR (188 MHz, acetone-D6): δ −73.8 (d, $^{1}J_{PF}$ = 706 Hz, PF₆) ppm. Anal. Calcd. for C₃₀H₁₈Cl₆CoF₁₂N₆P₂ (1224.08): C 35.18, H 1.77, N 8.21; found: C 36.58, H 1.76, N 8.25%.

[Co(Cl₂bpy)₃](PF₆)₃ (3b). 238 mg (1.0 mmol, 1 eq) of CoCl₂·6H₂O was dissolved in 15 mL of water and 675 mg (3.0 mmol, 3 eq) of 4,4′-dichloro-2,2′-bipyridine, dissolved in 60 mL of acetonitrile, was added. The solution instantly turned orange and was heated to 50 °C for 10 min. About 15 mL of acetonitrile was removed in vacuo. Then 4 mL of H₂O₂ (30%) and 4 mL of HCl (25%) were added. The mixture

was heated to 50 °C for 90 min. Excess of saturated aq. KPF_6 solution was added to precipitate the complex as its PF_6 salt. The solid was collected on a glass-frit, washed with water and Et_2O and dried *in vacuo*. The product was obtained as a pale green solid. Yield: 1.125 g (0.96 mmol, 96%). ^1H NMR (400 MHz, acetone-D6): δ 9.30 (t, $^4J_{HH}$ = 1.3 Hz, 6H, ArH), 7.97 (d, $^4J_{HH}$ = 1.3 Hz, 12H, ArH) ppm. ^{19}F NMR (188 MHz, acetone-D): δ −72.3 (d, $^1J_{PF}$ = 708 Hz, PF_6) ppm. HRMS (ESI-TOF) m/z (%): calcd. for $C_{30}H_{18}Cl_6CoF_6N_6P$ 438.9336; found 438.9354 (45) $[(M − 2PF_6)^{2+}]$; calcd. for $C_{30}H_{18}Cl_6CoN_6$ 244.3010; found 244.3019 (100) $[(M − 3PF_6)^{3+}]$. Anal. Calcd. for $C_{30}H_{18}Cl_6CoF_{18}N_6P_3$ (1169.05): C 30.82, H 1.55, N 7.19; found: C 31.04, H 1.35, N 7.35%.

[Co(bpy-pz)$_2$](B(CN)$_4$)$_2$ (5a). 0.29 g (1.2 mmol, excess) of $CoCl_2·6H_2O$ was dissolved in 8 mL of water while in another flask 0.44 g (2.0 mmol) of 6-(1H-pyrazol-1-yl)-2,2′-bipyridine (bpy-pz) was dissolved in 8 mL of acetone. The solutions were combined and heated to 50 °C for 20 min. To the solution, 460 mg of $KB(CN)_4$ dissolved in 15 mL of water was added. In addition 40 mL of water was added to force precipitation of the product. The solid was collected on a glass-frit and washed with water and Et_2O. The solid was dried *in vacuo* to obtain the pure product as a brown solid. Yield: 647 mg (0.88 mmol, 88%). ^1H NMR (400 MHz, acetone-D6): δ 114.72 (s, 2H, ArH), 94.40 (s, 2H, ArH), 91.55 (s, 2H, ArH), 77.09 (s, 2H, ArH), 70.87 (s, 2H, ArH), 68.66 (s, 2H, ArH), 43.88 (s, 2H, ArH), 41.05 (s, 2H, ArH), 19.50 (s, 2H, ArH), 14.00 (s, 2H, ArH) ppm. HRMS (ESI-TOF) m/z (%): calcd. for $C_{30}H_{20}BCoN_{12}$ 618.1364; found 618.1388 (100) $[(M − PF_6)^+]$; calcd. for $C_{26}H_{20}CoN_8$: 251.5571; found 251.5567 (96) $[(M − 2PF_6)^{2+}]$. Anal. Calcd. for $C_{34}H_{20}CoB_2N_{16}$ (733.19): C 55.70, H 2.75, N 30.57; found: C 55.83, H 2.74, N 30.01%.

[Co(bpy-pz)$_2$](B(CN)$_4$)$_3$ (5b). 0.12 g (0.5 mmol, excess) of $CoCl_2·6H_2O$ was dissolved in 6 mL of water while in another flask 0.15 g (0.66 mmol, 2eq) of 6-(1H-pyrazol-1-yl)-2,2′-bipyridine (bpy-pz) was dissolved in 3 mL of acetonitrile. The solutions were combined and heated to 50 °C for 20 min. Then 1.5 mL of H_2O_2 (30%) and 1.5 mL of HCl (37%) were added and the mixture was heated to 50 °C for 90 min. Approx. 0.2 g of $KB(CN)_4$ dissolved in 7 mL of water was added. In addition 20 mL of water was added to force precipitation of the product. The solid was collected on a glass-frit and washed with water and Et_2O. The solid was dried *in vacuo* to obtain the pure product as a orange solid. Yield: 125 mg (0.15 mmol, 44%). ^1H NMR (400 MHz, acetone-D6): δ 114.72 (s, 2H, ArH), 94.40 (s, 2H, ArH), 91.55 (s, 2H, ArH), 77.09 (s, 2H, ArH), 70.87 (s, 2H, ArH), 68.66 (s, 2H, ArH), 43.88 (s, 2H, ArH), 41.05 (s, 2H, ArH), 19.50 (s, 2H, ArH), 14.00 (s, 2H, ArH) ppm. HRMS (ESI-TOF) m/z (%): calcd. for $C_{34}H_{20}B_2CoN_{16}$ 733.1586; found 733.1617 (22) $[(M − B(CN)_4)^+]$; calcd. for $C_{26}H_{20}CoN_8$: 251.5571; found 251.5562 (100) $[(M − 2B(CN)_4)^{2+}]$. Anal. Calcd. for $C_{38}H_{20}B_3CoN_{20}··H_2O$ (866.08): C 52.70, H 2.56, N 32.34; found: C 52.46, H 2.26, N 32.17%.

[Co(bpy-pz)$_2$](TFSI)$_2$ (6a). 0.29 g (1.2 mmol, excess) of $CoCl_2·6H_2O$ was dissolved in 8 mL of water while in another flask 0.44 g (2.0 mmol) of 6-(1H-pyrazol-1-yl)-2,2′-bipyridine

(bpy-pz) was dissolved in 8 mL of acetone. The solutions were combined and heated to 50 °C for 20 min. To the solution, 650 mg of LiTFSI dissolved in water was added. The solid was collected on a büchner funnel and washed with a small amount of water and Et_2O. The solid was dried *in vacuo* to obtain the pure product as an orange solid. Yield: 767 mg (0.72 mmol, 72%). ^1H NMR (400 MHz, acetone-D6): δ 114.80 (s, 2H, ArH), 94.50 (s, 2H, ArH), 91.70 (s, 2H, ArH), 77.25 (s, 2H, ArH), 70.92 (s, 2H, ArH), 68.63 (s, 2H, ArH), 43.89 (s, 2H, ArH), 41.14 (s, 2H, ArH), 19.53 (s, 2H, ArH), 14.00 (s, 2H, ArH) ppm. ^{19}F NMR (188 MHz, acetone-D): δ −79.3 (s, $N(SO_2CF_3)_2$) ppm. HRMS (ESI-TOF) m/z (%): calcd. for $C_{28}H_{20}CoF_6N_9O_4S_2$ 783.0316; found 783.0333 (100) $[(M − N(SO_2CF_3)_2)^+]$. Anal. Calcd. for $C_{30}H_{20}CoF_{12}N_{10}O_8S_4$ (1063.72): C 33.87, H 1.90, N 13.17; found: C 34.34, H 1.74, N 12.82%.

[Co(py-py-pz)$_2$](TFSI)$_3$ (6b). 0.12 g (0.5 mmol, excess) of $CoCl_2·6H_2O$ was dissolved in 6 mL of water while in another flask 0.15 g (0.66 mmol, 2eq) of 6-(1H-pyrazol-1-yl)-2,2′-bipyridine (bpy-pz) was dissolved in 3 mL of acetonitrile. The solutions were combined and heated to 50 °C for 20 min. Then 1.5 mL of H_2O_2 (30%) and 1.5 mL of HCl (37%) were added and the mixture was heated to 50 °C for 90 min. Approx. 0.4 g of LiTFSI dissolved in 5 mL of water was added. In addition 25 mL of water was added to force precipitation of the product. The solid was collected on a glass-frit and washed with water and Et_2O. The solid was re-dissolved from the frit with acetone, concentrated and dried *in vacuo* to obtain the pure product as a brown solid. Yield: 364 mg (0.27 mmol, 82%). ^1H NMR (400 MHz, acetone-D6): δ 114.80 (s, 2H, ArH), 94.50 (s, 2H, ArH), 91.70 (s, 2H, ArH), 77.25 (s, 2H, ArH), 70.92 (s, 2H, ArH), 68.63 (s, 2H, ArH), 43.89 (s, 2H, ArH), 41.14 (s, 2H, ArH), 19.53 (s, 2H, ArH), 14.00 (s, 2H, ArH) ppm. HRMS (ESI-TOF) m/z (%): calcd. for $C_{30}H_{20}CoF_{12}N_{10}O_8S_4$ 1062.9489; found 1062.9470 (100) $[(M − N(SO_2CF_3)_2)^+]$. Anal. Calcd. for $C_{32}H_{20}CoF_{18}N_{11}O_{12}S_6$ (1343.87): C 28.60, H 1.50, N 11.46; found: C 28.63, H 1.63, N 10.98%.

3.3 Characterization of redox shuttles

Cyclic voltammetry experiments for the redox shuttle were realized at the same concentration of sample and electrolyte (0.1M $TBAPF_6$ in MeCN). Measurements were carried out in a glove box under an argon atmosphere using a set of Pt on FTO, Pt plate and Pt wire as working, counter and reference electrode, respectively. Ferrocene was used as internal standard and the voltage was sweep at a scan rate of 100 mV s^{-1} unless otherwise mentioned. Prior to each measurement, samples were stirred for 15s and left to equilibrate for 3s. ^1H NMR spectra were recorded using a Bruker AV 400 MHz spectrometer. Chemical shifts δ (in ppm) are referenced to residual solvent peaks. For ^1H NMR: acetone-D6, 2.05 ppm. ^{19}F and ^{31}P NMR were recorded using a Bruker AV 200 MHz spectrometer. Coupling constants are expressed in hertz (Hz). High-resolution mass spectra (HRMS) were obtained with a Waters Q-TOF-MS instrument using electrospray ionisation (ESI).

3.4 Counter electrode fabrication and characterization

The polymer was electrodeposited potentiostatically at a DC potential of +1.2 V using Eco Chemie AUTOLAB 1260 in a

three-electrode system comprised of working, platinum rod as the counter, and Ag/AgCl (leak free electrode procured from Harvard Apparatus GmbH) at 25 °C as the reference electrode. The potential was applied for a period of 20 s, unless otherwise stated in the text, sufficient enough to coat the TCO glass with polymer layers and to use them as metal free electro-catalyst. In the text PProDOT1 and PProDOT2 have been distinguished by the use of ionic liquids BMITFSI and EMIFAP, respectively. The working electrode, a SnO_2:F (FTO) coated glass plate ($\sim$15 Ω cm^{-2}, TEC-15, Solar 2.3 mm thickness), was placed parallel to the counter electrode in a solution containing the ionic liquids and 0.1 M monomer. The substrates were cleaned ultrasonically before use (in deionized water and ethyl alcohol) and kept in a solution of ethanol, and prior to use dried by blowing with dry air. After the polymerization process the film was washed repeatedly with isopropyl alcohol to get rid of any unreacted monomer or ionic liquids and annealed at 60 °C for 30 min. Scanning electron microscope (SEM) images were obtained with a low voltage SEM, LEO 1530 instrument and were imaged without coating. Conductive scanning force microscopy (CSFM) measurements were performed in contact mode (Multimode, Veeco, extended with a TUNA current amplifier module for current measurements). Pt/Ir coated probes were used (Nanosensors PPP-EFM-50, 70 kHz) for CSFM experiments. The sample was glued with silver paste on a conductive steel substrate and to avoid electromagnetic noise, the scanner was shielded by wrapping Al foil around the SFM recording setup, and minimum possible force was applied to minimize possible destruction of the surface.

3.5 Solar cell fabrication and characterization

FTO glass plates (Nippon Sheet Glass, Solar 4 mm thickness) were dipped in 40 mM $TiCl_4$ aq. at 70 °C for 30 min and washed with water and ethanol. A paste composed of 20 nm anatase TiO_2 particles for the transparent nanocrystalline layer was coated on the FTO glass plates by screen printing. The TiO_2 electrodes were made of $\sim$11 μm transparent layer (20 nm) and $\sim$5 μm scattering layer (400 nm, CCIC, HPW-400). The TiO_2 electrodes were gradually heated under an air flow. After a second $TiCl_4$ treatment, the TiO_2 electrodes were immersed into a dye solution 3-{6-{4-[bis(2′,4′-dihexyloxybiphenyl-4-yl)amino-]-phenyl}-4,4-dihexyl cyclopenta-[2,1-b:3,4-b′]dithiophene-2-yl}-2-cyanoacrylic acid, (labelled as **Y123**)[15] in a 50/50 (v/v) mixture of acetonitrile and tert-butanol and kept at room temperature for 18 h. The dye-coated TiO_2 photoanode and counter electrode were assembled into a sealed sandwich type cell with a gap of a hot-melt ionomer film, Surlyn (25 μm, Du-Pont). To reduce scattered light from the edge of the glass electrodes of the dyed TiO_2 layer, a light shading mask was used on the DSSCs, so the active area of DSSCs was fixed to 0.2 cm^2. Photovoltaic experiments were made according to the reported method[5,22] and the measurement settling time between applying a voltage and measuring a current for the I–V characterization of DSSCs was fixed to 40 ms at an interval of 10 mV.

4. Conclusions

We have synthesized a series of cobalt complexes with various polypyridyl ligands to rival I_3^-/I^- application. The rational design allows us to tune the oxidation potential from 0.17 to 0.34 V vs. ferrocene by using electron acceptor groups. Since the platinized cathode was not effective, with the newly developed cobalt based redox shuttle, the introduction of alternative platinum-free cathodes based on poly(alkylthiophenes) resulted in enhanced PV properties. By using electrodeposited PProDOT as a cathode, we are able to improve the performance (by more than 20%) for these systems. The enhanced PV performance originates from the 3-dimensional ultra-porous microstructure with high surface area of the polymer cathode. These nanoporous polymer films will possibly eliminate the formation of any passivation layer at the interface as observed by charge transfer resistance value. By the use of different ionic liquids the pore size and microstructure of polymer layers can be easily tuned for optimum results. With the combination of a transparent and noncorrosive cobalt (III/II) redox shuttle with a cheap electrocatalyst, the reported system shows great potential for large-scale DSSCs fabrication.

References

1 B. E. Hardin, H. J. Snaith and M. D. McGehee, *Nat. Photonics*, 2012, **6**, 162–169.
2 A. Hagfeldt, G. Boschloo, L. Sun, L. Kloo and H. Pettersson, *Chem. Rev.*, 2010, **110**, 6595–6663.
3 B. E. Hardin, A. Sellinger, T. Moehl, R. Humphry-Baker, J.-E. Moser, P. Wang, S. M. Zakeeruddin, M. Graetzel and M. D. McGehee, *J. Am. Chem. Soc.*, 2011, **133**, 10662–10667.
4 K. Do, D. Kim, N. Cho, S. Paek, K. Song and J. Ko, *Org. Lett.*, 2012, **14**, 222–225.
5 J.-H. Yum, E. Baranoff, F. Kessler, T. Moehl, S. Ahmad, T. Bessho, A. Marchioro, E. Ghadiri, J.-E. Moser, C. Yi, M. K. Nazeeruddin and M. Grätzel, *Nat. Commun.*, 2012, **3**, 631.
6 H. Tian, E. Gabrielsson, Z. Yu, A. Hagfeldt, L. Kloo and L. Sun, *Chem. Commun.*, 2011, **47**, 10124–10126; J. Burschka, V. Brault, S. Ahmad, L. Breau, M. K. Nazeeruddin, B. Marsan, S. M. Zakeeruddin and M. Grätzel, *Energy Environ. Sci.*, 2012, **5**, 6089–6097.
7 N. Papageorgiou, *Coord. Chem. Rev.*, 2004, **248**, 1421–1446.
8 H. Nusbaumer, J.-E. Moser, S. M. Zakeeruddin, M. K. Nazeeruddin and M. Grätzel, *J. Phys. Chem. B*, 2001, **105**, 10461–10464.
9 S. A. Sapp, C. M. Elliott, C. Contado, S. Caramori and C. A. Bignozzi, *J. Am. Chem. Soc.*, 2002, **124**, 11215–11222.
10 H. Nusbaumer, S. M. Zakeeruddin, J. E. Moser and M. Grätzel, *Chem.–Eur. J.*, 2003, **9**, 3756–3763.
11 H. X. Wang, P. G. Nicholson, L. Peter, S. M. Zakeeruddin and M. Grätzel, *J. Phys. Chem. C*, 2010, **114**, 14300–14306.
12 P. J. Cameron, L. M. Peter, S. M. Zakeeruddin and M. Grätzel, *Coord. Chem. Rev.*, 2004, **248**, 1447–1453.

13 S. M. Feldt, E. A. Gibson, E. Gabrielsson, L. Sun, G. Boschloo and A. Hagfeldt, *J. Am. Chem. Soc.*, 2010, **132**, 16714–16724.

14 T. W. Hamann and J. Wondersma, *Energy Environ. Sci.*, 2011, **4**, 370–381.

15 H. N. Tsao, C. Yi, T. Moehl, J.-H. Yum, S. M. Zakeeruddin, M. K. Nazeeruddin and M. Grätzel, *ChemSusChem*, 2011, **4**, 591–594.

16 H. N. Tsao, J. Burschka, C. Yi, F. Kessler, M. K. Nazeeruddin and M. Grätzel, *Energy Environ. Sci.*, 2011, **4**, 4921–4924.

17 M. J. J. Mulder, J. G. Haasnoot, D. J. Stufkens, L. H. Tjeng, H.-J. Lin, C.-T. Chen and J. Reedijk, *Eur. J. Inorg. Chem.*, 2002, 3083–3086.

18 B. W. -Jensen and D. R. MacFarlane, *Energy Environ. Sci.*, 2011, **4**, 2790–2798.

19 S. Ahmad, M. Deepa and S. Singh, *Langmuir*, 2007, **23**, 11430–11433.

20 S. Ahmad, R. Berger, H. U. Khan and H.-J. Butt, *J. Mater. Chem.*, 2010, **20**, 5325–5334.

21 Y. Liu, J. R. Jennings, M. Parameswaran and Q. Wang, *Energy Environ. Sci.*, 2011, **4**, 564–571.

22 S. Ahmad, J.-H. Yum, Z. Xianxi, M. Grätzel, H.-J. Butt and M. K. Nazeeruddin, *J. Mater. Chem.*, 2010, **20**, 1654–1658; S. Ahmad, J.-H. Yum, H.-J. Butt, M. K. Nazeeruddin and M. Grätzel, *ChemPhysChem*, 2010, **11**, 2814–2819.

23 K. M. Lee, P. Y. Chen, C. Y. Hsu, J. H. Huang, W. H. Ho, H. C. Chen and K. C. Ho, *J. Power Sources*, 2009, **188**, 313–318; K. M. Lee, C. Y. Hsu, P. Y. Chen, M. Ikegami, T. Miyasaka and K. C. Ho, *Phys. Chem. Chem. Phys.*, 2009, **11**, 3375–3379.

24 E. Palomares, J. N. Clifford, S. A. Haque, T. Lutz and J. R. Durrant, *J. Am. Chem. Soc.*, 2003, **125**, 475–482; J. H. Yum, S. J. Moon, R. Humphry-Baker, P. Walter, T. Geiger, F. Nuesch, M. Grätzel and M. K. Nazeeruddin, *Nanotechnology*, 2008, **19**, 424005.

25 J. D. Stenger-Smith, C. K. Webber, N. Anderson, A. P. Chafin, K. Zong and J. R. Reynolds, *J. Electrochem. Soc.*, 2002, **149**, A973–A977.

26 J. Burschka, A. Dualeh, F. Kessler, E. Baranoff, N.-Lê Cevey-Ha, C. Yi, M. K. Nazeeruddin and M. Grätzel, *J. Am. Chem. Soc.*, 2011, **133**, 18042–18045.